Phosphotyrosine Profiling of NSCLC Cells in Response to EGF and HGF Reveals Network Specific Mediators of Invasion

Citation: Johnson, Hannah, Rebecca S. Lescarbeau, Jesus A. Gutierrez, and Forest M. White. "Phosphotyrosine Profiling of NSCLC Cells in Response to EGF and HGF Reveals Network Specific Mediators of Invasion." Journal of Proteome Research 12, no. 4 (April 5, 2013): 1856–1867.

As Published: http://dx.doi.org/10.1021/pr301192t

Publisher: American Chemical Society (ACS)

Persistent URL: http://hdl.handle.net/1721.1/89044

Version: Author's final manuscript: final author's manuscript post peer review, without publisher's formatting or copy editing

Published in final edited form as:
J Proteome Res. 2013 April 5; 12(4): 1856–1867. doi:10.1021/pr301192t.

Phosphotyrosine Profiling of NSCLC cells in Response to EGF and HGF Reveals Network Specific Mediators of Invasion

Hannah Johnson[1,2], **Rebecca S. Lescarbeau**[1,2], **Jesus A. Gutierrez**[3], and **Forest M. White**[1,2,*]

[1]Department of Biological Engineering, Massachusetts Institute of Technology, Cambridge, MA, USA

[2]Koch Institute for Integrative Cancer Research, Massachusetts Institute of Technology, Cambridge, MA, USA

[3]Tailored Therapeutics, Lilly Research Laboratories, Eli Lilly and Company, Indianapolis, IN, USA

Abstract

Growth factor signaling is deregulated in cancer and often leads to invasion, yet receptor tyrosine kinase signaling pathways driving invasion under different growth factor conditions are not well understood. To identify specific signaling molecules regulating invasion of A549 non-small cell lung carcinoma (NSCLC) cells downstream of the epidermal growth factor receptor (EGFR) and Met, quantitative site specific mass spectrometric analysis of tyrosine phosphorylation was performed following epidermal growth factor (EGF) or hepatocyte growth factor (HGF) stimulation, at three different growth factor concentrations and at two time points. Through this analysis the temporal and concentration dependent phosphorylation profiles were obtained for 131 sites and 139 sites downstream of EGF and HGF stimulation, respectively. To characterize the effect of these signaling network alterations, we quantified 3D cell migration/invasion through Matrigel. Partial least squares regression (PLSR) analysis was performed to identify the tyrosine phosphorylation sites most strongly correlated with EGF and/or HGF mediated invasion. Potential common and specific signaling events required for driving invasion downstream of EGFR and Met were identified using either a combined or two independent PLSR models, based on the quantitative EGF or HGF data. Our data highlight the integration and compartmentalization of signaling required for invasion in cancer.

Keywords

Cancer; Proteomics; Invasion; Tyrosine Phosphorylation; Quantification; iTRAQ

INTRODUCTION

The role of HGF and EGF driven signaling in invasion and migration in cancer pathogenesis has long since been established [1, 2]. Binding of HGF to the receptor tyrosine kinase (RTK) encoded by the c-Met proto-oncogene [3–5] leads to dimerization and activation through phosphorylation on tyrosine residues in the intracellular kinase domain of the receptor [6].

*Corresponding Author, Forest M. White, 77 Massachusetts Ave, 76-353, Cambridge MA 02139, Phone: (617) 258-8949, Fax: (617) 452-4978 fwhite@mit.edu.

Author Contributions

The manuscript was written through contributions of all authors. All authors have given approval to the final version of the manuscript.

Kinase activation leads to trans-autophosphorylation on tyrosine residues in the cytoplasmic tail. These phosphorylation events form docking sites allowing adaptor molecules such as Gab1, Grb2, PLC-γ, and Src to bind and perpetuate downstream signaling, eventually leading to cellular phenotypes such as migration, invasion and proliferation [7, 8]. HGF signaling through Met is known to play a significant role in promoting tumor cell invasion and metastasis in several different cell types such as lung and pancreatic carcinomas [9, 10]. Deregulated Met signaling has been implicated in NSCLC and disruption of this pathway by Met-directed inhibitors decreases tumorigenic potential, yet these inhibitors have been prone to failure due to adaptation of the tumor microenvironment [11].

EGFR is an RTK that binds EGF to cause dimerization, trans-autophosphorylation, activation, and downstream signaling [12]. Similar to Met, EGFR activation leads to phosphorylation of specific tyrosine residues within the cytoplasmic tail that serve as docking sites for proteins containing Src homology 2 (SH2) and phosphotyrosine binding (PTB) domains, the recruitment of which leads to activation of intracellular signaling pathways [13–15]. Signaling downstream of EGFR regulates proliferation, migration, and invasion [16]. Due to its increased activity in several cancers, including NSCLC, EGFR has emerged as a therapeutic target [16]. Despite the high efficacy of EGFR tyrosine kinase inhibitors (TKIs) such as gefitinib and erlotinib, innate or adaptive resistance associated with compensatory signaling through additional RTKs has been detected in almost all cases [16]. Met is frequently co-expressed with EGFR family members in human tumors and cross-talk between these RTKs have been described in several contexts, including invasive growth [17–20]. Aberrant EGFR activation increases protein expression and phosphorylation of Met in thyroid carcinoma and gliobastoma cell lines [21, 22]. Furthermore, characterization of phosphotyrosine signaling downstream of the EGFR receptor in NSCLC cell lines and Met in a gastric cancer cell line demonstrated increased phosphorylation of EGFR in a Met amplified cell line and increased Met phosphorylation in mutated and amplified EGFR cell lines [23]. Additionally, inhibition of EGFR signaling with EGFR TKIs can lead to compensatory signaling through Met [19]. These studies demonstrate cross-talk between EGFR and Met signaling in driving invasive cancer progression, yet the specific and common nodes involved in these networks have not yet been characterized at a systems level.

Although the extent to which the EGF and HGF signaling pathways overlap is not fully understood, many of the canonical adaptor proteins and downstream pathways are known to be common to both receptors. To determine the overlap between these networks, a recent study utilized quantitative mass spectrometric analysis of proteins following phosphotyrosine immunoprecipitation after stimulation with EGF or HGF [24]. While a significant number of common proteins were immunoprecipitated after EGF and HGF stimulation, phosphorylation site-specific information was lacking, and therefore it was unclear as to whether both networks phosphorylated the same sites on these proteins.

In this study, to determine EGF and HGF network specific mediators of invasion we characterized temporal site-specific phosphotyrosine signaling in A549 cells by quantitative mass spectrometry. We quantified invasion and tyrosine phosphorylation signaling networks at four growth factor concentrations determined using a standard Boyden chamber invasion assay; EC_0 (no growth factor), EC_{50} (the effective concentration that results in 50% of the maximum invasion), EC_{100} (the effective concentration that results in 100% i.e. maximum invasion), and EC_{am50} (the effective concentration above EC_{100} that results in 50% of the maximum invasion). These analyses led to the identification and quantification of 131 phosphotyrosine peptides following EGF stimulation and 139 phosphotyrosine peptides following HGF stimulation; a total of 78 phosphorylation sites were quantified across all EGF and HGF stimulation conditions. Integration of the quantitative temporal

phosphotyrosine data enabled us to calculate the total signal from 0 to 20 minutes and correlate these measurements to invasion using PLSR. Through these efforts, we have uncovered phosphorylation sites correlated with invasion and highlight both common and differential tyrosine phosphorylation sites regulating invasion downstream of EGFR and Met.

MATERIALS AND METHODS

Cell Culture

The lung adenocarcinoma cell line A549 was grown in RPMI-1640 medium with glutamine supplemented with 10% fetal bovine serum in a humidified incubator at 37 °C with 5% CO_2. Prior to sample preparation for mass spectrometry, cells were serum starved for 24 h using RPMI-1640 supplemented with 0.1% BSA then stimulated with the indicated concentrations of either EGF or HGF for the appropriate time periods.

Cell Invasion Assay

In vitro invasion of A549 cells was performed using 8.0 μm pore size Transwell cell culture inserts coated with 5μg Matrigel (BD Biosciences). Prior to the assay, cells were serum depleted for 24 h in RPMI-1640 supplemented with 0.1% BSA. Cell suspensions containing 5×10^5 cells were seeded into the upper region of a Boyden chamber. RPMI-1640 containing EGF, HGF, or 10% FBS was then placed in the lower chamber. Cells were allowed to invade through the Matrigel-coated membrane for 20 h, after which the cells on the filter were stained with 0.1% crystal violet and scanned into Image J. Invasive cells on the bottom of the membrane were then quantified using Image J software. Percent invasion was calculated relative to invasion induced by 10% FBS and EC_0, EC_{50}, EC_{100} and EC_{am50} were determined for EGF and HGF.

Cell Lysis

Cells were lysed in ice-cold 8M urea for mass spectrometric analyses or modified RIPA buffer for immunoblotting supplemented with 1mM sodium orthovanadate, 0.1% NP-40, and protease and phosphatase inhibitor cocktail tablets (Roche). Protein concentrations were quantified using BCA assay (Pierce).

Immunoblotting

Cell lysates were separated on a 7.5% polyacrylamide gel and electrophoretically transferred to nitrocellulose (Biorad). Nitrocellulose was blocked with 5% BSA in TBS-T (150mM NaCl, 0.1% Tween 20, 50 mM Tris, pH 8.0). Antibodies used are as follows: anti-EGFR (BD Biosciences), anti-EGFR pY1173 (Epitomics), anti-c-Met (Epitomics), anti-c-Met pY1234/5 (Epitomics), anti-phosphotyrosine (4G10, Millipore), and anti-β-tubulin (Cell Signaling Technology). Antibodies were diluted in blocking buffer and incubated with nitrocellulose overnight at 4°C. Secondary antibodies (either goat anti-rabbit or goat anti-mouse conjugated to horseradish peroxidase) were diluted 1/10,000 in TBS-T and incubated at room temperature for 1 h. Antibody binding was detected using the enhanced chemiluminescence (ECL) detection kit (Pierce).

Mass Spectrometry Sample Preparation

Proteins were reduced (10 mM DTT, 56°C for 45 min), alkylated (50mM iodoacetamide, room temperature in the dark for 1 h), and excess iodoacetamide was quenched with DTT to a final concentration of 25 mM. Proteins were subsequently digested with trypsin (sequencing grade, Promega), at an enzyme/substrate ratio of 1:100, at room temperature overnight in 100mM ammonium acetate pH 8.9. Trypsin activity was quenched by adding

formic acid to a final concentration of 5%. Urea was removed from the samples by reverse phase desalting using a C18 cartridge (Waters) and peptides were lyophilized and stored at −80°C.

iTRAQ Labeling

Peptide labeling with iTRAQ 8plex (AB Sciex) was performed as previously described [25]. Growth factor stimulated A549 cells were labeled using the iTRAQ 8plex channels as follows: 113-EC_0; 114-EC_{50}(5min); 115-EC_{100}(5min); 116-EC_{am50}(5min); 117-EC_{50}(20min); 118-EC_{100}(20min); 119-EC_{am50}(20min); and 121-10% FBS for EGF or HGF. Three biological replicates were performed for each of the EGF and HGF stimulation conditions.

Phosphotyrosine Enrichment

Phosphotyrosine peptides were enriched prior to mass spectrometry analyses using a cocktail of anti-phosphotyrosine antibodies followed by immobilized metal affinity chromatography (IMAC) as previously described [26]. Peptides retained on the IMAC column were eluted to a C18 reverse-phase pre-column (100 μm ID, 10 cm packed bed length, YMC ODS-A, 10 μm), which was then rinsed with 0.1% acetic acid to remove excess phosphate buffer. After rinsing, the precolumn was attached to a C18 reverse-phase analytical column (50 μm ID, 10 cm packed bed length, YMC ODS-AQ, 5 μm) with integrated electrospray emitter tip. Peptides were chromatographically separated by reverse phase HPLC (Agilent) over a 140 minute gradient (buffer A = 200 mM acetic acid, buffer B = 70% acetonitrile in 200 mM acetic acid; 0-10 min: 13%, 10-105 min: 42%, 105-115 min: 60%, 115-122 min: 100%, 122-128 min: 100%, 128-130 min: 0%, 130-150 min: 0%,) and nano-electrosprayed directly into an Orbitrap XL mass spectrometer (Thermo Scientific). The mass spectrometer was operated in data-dependent mode with a full scan MS spectrum followed by MS/MS (CID was set at 35% energy for sequence information and HCD at 75% energy for iTRAQ quantification) for the top 10 precursor ions in each cycle. Ion trap injection time was set to 100 ms and FTMS injection time was set to 1000 ms with a resolution of 60000 across *m/z* 400-2000. For IT and FT-MS/MS scans, fragmentation was carried out on ions above a threshold of 500 counts and an FTMS resolution of 7500.

Phosphotyrosine Data Analysis

Raw mass spectral data files (.RAW files) were converted into .mgf file format using DTAsupercharge 1.31 (http://msquant.sourceforge.net/). All resulting MS/MS peak lists were searched against a UniProt database containing *Homo sapiens* protein sequences (37,743 entries) using Mascot (Matrix Science, version 2.1.03). Briefly, trypsin enzyme specificity was applied with a maximum of 1 missed cleavage. Mass tolerance for precursor ions was set to 10 ppm, and fragment ion mass tolerance was 0.8 Da. MS/MS spectra searches incorporated fixed modifications of carbamidomethylation of cysteine and iTRAQ 8plex modification of lysines and peptide N-termini. Variable modifications were oxidized methionine, and phosphorylation of serine, threonine, and tyrosine residues. Phosphotyrosine peptides were initially filtered using a Mascot score cut-off of 20, which corresponds to an FDR of 3 % at the peptide level. Precursor ions were manually evaluated and peptides with contaminating peaks present within the isolation window (ions with intensity > 25% of the base peak ± 1.5 *m/z* around the selected precursor ion m/z) were discarded as they may contribute to the relative iTRAQ intensities. MS/MS spectra of the tyrosine phosphorylated peptides were manually validated to confirm peptide identification and phosphorylation site localization. Manually annotated spectra of the 131 phosphotyrosine peptides identified after EGF stimulation and 139 phosphotyrosine peptides identified after HGF stimulation can be found in Supplementary Figures 1 and 2

respectively. EGFR phosphorylation site numbering excludes the 24 amino acid signal peptide sequence. iTRAQ intensity values were extracted from HCD scans using an in house python script which converted iTRAQ intensities into .txt format. To determine the relative phosphorylation level of each phosphosite, the iTRAQ quantification data were corrected for isotopic overlap, as previously determined by AB Sciex, normalized to total protein signal of each sample, and normalized to the 10% FBS condition for both the EGF and HGF experiments. To quantify the overall phosphorylation signal for each peptide at EC_0, EC_{50}, EC_{100} and EC_{am50}, the area under the curve (AUC) was calculated using relative intensities at 0, 5 and 20 minutes post growth factor stimulation. The normalized signal across time was integrated from EC_0 (set as our initial measurement) to the 5 min and 20 min phosphorylation level at each concentration prior to PLSR.

Affinity Propagation Clustering Analysis

Affinity propagation clustering was carried out as previously described [26].

Partial least square regression

The PLSR model was generated using SIMCA-P (11.5) as previously described [27]. Briefly, an MxN matrix (X) was generated from the AUC (0 to 20 min) quantified for each of the phosphorylation sites generated from the mass spectrometric data. Each of the M rows corresponded to a different treatment: EGF EC_0, EGF EC_{50}, EGF EC_{100}, EGF EC_{am50}, HGF EC_0, HGF EC_{50}, HGF EC_{100}, and HGF EC_{am50}. Each of the N columns corresponded to one phosphorylated peptide that was measured in either or both the EGF stimulation and the HGF stimulation datasets. A vector (Mx1, Y) was generated that described the invasion (cellular output). The M rows in the vector of Y corresponded to the same cellular conditions as in X. The invasion data and quantitative data for each phosphorylated peptide were mean centered across the cellular conditions and then Log_2 transformed. Models were generated using three principal components (combined EGF and HGF model) or two principal components (individual EGF or HGF models) under the standard optimization criteria. The nonlinear iterative partial least-square algorithm was used to solve the equation $Y=bX+e$, where b is a vector of regression coefficients and e is the residual, such that that $X=t1p1'+t2p2'+\ldots+e$ where each t is a new, latent score variable onto which the original data can be projected, creating a principal component, and where each score is orthogonal to every other. This equation maximizes the covariance of linear combinations of the phosphorylated peptides (i.e. scores) to the response, invasion (with the first principal component capturing the most variation in the data and each sequential score vector correlating the X matrix to the y-residual of the previous score vector, or the entire Y vector for the first score vector). The ps in the equation are the coefficients that map each phosphosite onto each principal component. The variable importance in the projection (VIP) score was used to identify explanatory variables that contribute the most to the prediction of invasion in response to EGF or HGF in A549 cells.

RESULTS AND DISCUSSION

Characterization of A549 cell invasion in response to EGF or HGF

To verify protein expression levels of EGFR and Met in the A549 cells, immunoblotting was carried out for total EGFR or Met (Figure 1A). The protein expression of EGFR and Met was not affected by EGF or HGF stimulation at 30 min. While EGF stimulation increased EGFR Y1173 phosphorylation and HGF stimulation increased Met Y1234/5 phosphorylation, EGF stimulation did not increase Met Y1234/5 phosphorylation, and HGF did not increase EGFR Y1173 phosphorylation (Figure 1A). This result demonstrated that there was minimal crosstalk at the receptor level in terms of tyrosine phosphorylation in these cells under these conditions. To confirm that the signaling networks downstream of

both receptors were functional under these stimulation conditions, we immunoblotted cell lysates for total phosphotyrosine after stimulation with EGF or HGF (Figure 1A). We observed a global increase in tyrosine phosphorylation in response to EGF and HGF, but did not identify any significant differences between the two growth factors other than the receptors at 180kDa (EGFR) and 120kDa (Met). To quantify the cell biological response to stimulation of these cells with EGF or HGF, we carried out Boyden chamber invasion assays using Matrigel coated membranes. Invasion through Matrigel was quantified in response to 7 different EGF concentrations (Figure 1B) and 7 different HGF concentrations (Figure 1C) in comparison to 10% FBS. The invasion of A549 cells in response to EGF and HGF was quantitatively distinct, and the level of growth factor required to induce maximal invasion was much higher for HGF (300 ng/ml= 3.7 nM) versus EGF (10 ng/ml= 1.6 nM). These data allowed us to identify the effective concentrations for invasion in A549 cells.

Quantification of signaling in A549 cells in response to EGF or HGF

To determine the phosphorylation signaling networks driving invasion under EGF or HGF stimulation conditions, the EC_0, EC_{50}, EC100 and EC_{am50} were selected for phosphotyrosine signaling analysis using quantitative mass spectrometry. Cells were stimulated for 5 or 20 minutes with the indicated effective concentrations or 10% FBS, which was used as a control. Cells were lysed with 8 M urea and proteins were reduced, alkylated and digested with trypsin prior to differential labeling with iTRAQ8plex reagent and liquid chromatography tandem mass spectrometry (LC-MS/MS) analysis (Figure 2). To calculate the total signal for each effective concentration, we calculated the area under the curve (AUC) using the EC_0 as the 0 minute and the 5 and 20 minute time points for EC_{50}, EC_{100} and EC_{am50}. The basal level of phosphorylation was calculated by extrapolating the level of the EC_0 0 minute measurement out to 5 and 20 minutes and calculating the AUC. In total, 131 phosphotyrosine peptides in the EGF dataset and 139 phosphotyrosine peptides in the HGF dataset were identified and quantified across 3 different effective concentrations at 2 different time points. iTRAQ quantification information along with the peptide sequence and phosphorylation site localization can be found in Supplementary table 1 and Supplementary table 2, respectively. To identify phosphorylation sites that were either EGF or HGF responsive, we filtered the quantitative information for those peptides with a ≥1.5 fold change relative to EC_0 in any of the growth factor iTRAQ channels. This threshold was determined as the median coefficient of variation was found to be 15.7 % for EGF analyses and 14.4 % for HGF analyses, thus ≥1.5 fold changes are statistically different. This filtering resulted in 68 EGF responsive phosphorylation sites and 61 HGF responsive phosphorylation sites. To define sets of similarly regulated phosphorylation sites, responsive sites were clustered using affinity propagation, and are displayed as heat maps in Figure 3A and 3B. As expected, stimulation of A549 cells with EGF resulted in a robust phosphorylation increase on EGFR Y1173 and Y1148 along with known immediate downstream signaling proteins such as Gab1, Shc1, and INPPL1 (Ship2) [13]. Overall the response to HGF stimulation was more muted than EGF, and the phosphorylation sites with the largest response were those at the receptor and those known to signal directly downstream of Met such as Gab1, GRB2, and Ship2 [28]. EGFR phosphorylation on Y1068 and Y1173 both increased by approximately 1.5 fold following HGF stimulation, despite no perceptible increase in phosphorylation of these sites in the immunoblot data in Figure 1A. This difference is likely due to the fold-change of 1.5 fold that was detected by mass spectrometry being below the limits of detection of immunoblotting in this instance. Several EGF and HGF responsive phosphorylation sites were identified on proteins known to be involved in cell adhesion, migration, and invasion. For instance, phosphorylation of Y30 and Y188 on Annexin A2 (ANXA2) and Y780, Y823, Y855, Y333/Y354 on tensin 3 (TNS3) were identified as EGF and HGF responsive. ANXA2 has been shown to play an important role in tumor progression and invasion in gliomas and ovarian cancers, and TNS3 is known

to inhibit cell migration in breast and kidney cancer, yet the role of the phosphorylation sites identified here is not known [29–32].

To visualize the effect of EGF and HGF stimulation on the signaling pathways downstream of the receptors, we mapped the responsive phosphorylation sites to a canonical network diagram (Figure 3C), where EGF responsive phosphotyrosine sites are represented in blue and HGF responsive phosphotyrosine sites are green. Phosphorylation sites on PLC-γ and Crk were detected in the EGF responsive dataset and it is known that Crk and PLC-γ play a role in signaling downstream of EGFR [13, 33]. PLC-γ and Crk are also involved in Met signaling but were not detected in the HGF dataset [28]. HGF resulted in responsive phosphorylation across multiple RTKs with AXL, FGFR, and IGF1R phosphorylation sites increasing in response to HGF stimulation, thus indicating crosstalk between these receptors. These data demonstrate distinct qualitative differences in the EGF and HGF signaling networks.

Correlation of EGF and HGF phosphotyrosine signaling to invasion with a combined PLSR model

To identify the common signaling pathways mediating invasion downstream of EGFR and Met, we selected the 78 overlapping phosphorylation sites that were quantified across both the EGF and HGF datasets. The calculated AUC measurements for the 3 EGF or HGF effective concentrations in addition to the EC_0 are displayed in a heat map in Figure 4A. It is important to note that while the EC_0 measurements should theoretically be identical, some variation in selected phosphorylation sites can be seen across the different biological replicates. Despite this biological variation, distinct differences in signaling between EGF and HGF were detectable (Figure 4A). To identify the sites most strongly correlated with invasion downstream of EGFR or Met activation, the 78 common phosphorylation sites were regressed against the quantitative invasion data at each of the effective concentrations using PLSR. The PLSR model contained 3 principal components, which explained 89 % of the variation in the data. Figure 4B displays the scores plot of principal component 1 and 2 (PC1 and PC2) from the resulting model; EGF data are highlighted in blue and the HGF data are highlighted in green. Principal component 1 discriminated the data based on increasing invasion following growth factor stimulation, where A549 cells stimulated with EC_{100} separated from the EC_{50} and EC_{am50} cells. Principal component 2 discriminated the data based on the differential quantitative invasion profiles resulting from the 2 different growth factors, where EGF and HGF data points separate. Phosphorylation sites with the lowest coefficients on PC2 were HGF specific phosphorylation sites such as Gab1 (Y406 and Y689), Lyn (Y316), PTPRA (Y798), intersectin2 (ITSN2; Y940) and MPP5 (Y243). EGF specific phosphorylation sites defined by the highest coefficients were EGFR (Y1173), Lyn (Y397), Ship2 (Y986 and Y1135), MAPK1 (ERK2) (Y187/T185), Shc1 (Y349/Y350) and BCAR1 (p130Cas; Y249). While many of these phosphorylation sites have not been previously attributed specifically to the EGF or HGF signaling networks, these data suggest specific mediation of these phosphorylation sites downstream of the respective receptors.

To identify the quality of the combined model, we calculated the linear regression of the measured invasion versus the predicted invasion and identified an R_2 value of 0.8881 (Figure 4C). PLSR predicted invasion via a linear regression of the datasets in a reduced-dimensionality principal component space with regression coefficients associated with principal components. To identify phosphotyrosine sites that correlated most highly to the prediction of invasion in response to either EGF or HGF in A549 cells, phosphorylation sites with VIP scores above 1 were selected and are listed in Figure 4C. Phosphotyrosine sites at the top of the canonical signaling networks (e.g. EGFR, Met, Gab1, Shc1, Ship2, ERK1 (MAPK3), and ERK2) were most important in driving the phenotypic response in this combined model. These sites are the primary docking and activation sites that mediate

downstream network activity, so while their correlation with invasion was expected, this result highlights the power of the model to identify crucial nodes in the network. Several less well characterized phosphorylation sites (e.g. Csk Y184, intersectin2 Y940, Cbl Y371, calmodulin (CALM1) Y100, ANXA2 Y188, and TNS3 Y333/Y354) were also found to be strongly correlated with invasion in this model. Further work is needed to determine the mechanistic contribution of these phosphorylation events to invasion downstream of HGF or EGF stimulation of these cells.

Identification of EGF and HGF specific mediators of invasion

To parse out differences in EGF and HGF signaling in relation to invasion in A549 cells, we used the EGF and HGF datasets individually to specifically identify phosphorylation sites correlated with invasion after EGF or HGF stimulation. We built an EGF-only model with the quantitative data from the 78 overlapping phosphorylation sites shown in Figure 4A. The top 26 phosphorylation sites that contributed most significantly to the model are shown in Figure 5A along with their respective VIP scores. We generated a reduced 'EGF-only' model, based on these 26 sites, which was then used to predict invasion. The predictive power of the reduced EGF model was the same as the full 78 phosphorylation site EGF model, with both models displaying an R^2 value of 0.9982 (Figure 5B). To identify how specific these 26 phosphorylation sites were for predicting the pattern of EGF driven invasion, we used the reduced EGF model to predict invasion following HGF stimulation. Intriguingly, the EGF-only reduced model could not predict the measured HGF invasion (R^2 = 0.0686) (Figure 5C). To ensure that this reduction in the predictive power of the model was not solely due to the receptor we removed EGFR from the model. A model comprised of the remaining 25 phosphorylation sites still failed to predict HGF invasion (R^2 = 0.2925). To identify HGF specific mediators of invasion, we built a HGF-only model with the quantitative data from the 78 overlapping phosphorylation sites shown in Figure 4A. The top 26 phosphorylation sites that contributed most significantly to the model were again selected (Figure 5D) and used to generate a reduced 'HGF-only' model. The predictive power of the reduced HGF model was similar to the full 78 phosphorylation site HGF model, with the full model demonstrating an R^2 value of 0.9735 and the reduced model providing an R^2 value of 0.9572 (Figure 5E). To confirm the specificity of these 26 phosphorylation sites for predicting HGF driven invasion, we used the reduced HGF model to predict EGF invasion. The HGF data also performed poorly at predicting the measured EGF invasion (R^2 = 0.3200) (Figure 5F). To assess the role of Met in affecting the model specificity, we removed Met from the model. A model comprised of the resulting 25 phosphorylation sites could still not predict EGF invasion (R^2= 0.2716). It is worth noting that the same 78 phosphorylation sites were used in both of the individual models. The difference between the models is therefore not due to qualitatively different sites, but is instead due to the quantitative differences in site-specific phosphorylation associated with the distinct growth factor stimulations. Since the same sites were used to construct both models, the two individual models can be directly compared to determine the contribution of specific phosphorylation sites to each model.

Specific EGF mediators are highlighted in Figure 5A with asterisks. Several of these proteins have been previously associated with cell migration and/or invasion, including ELMO2, involved in cytoskeletal rearrangement and cell motility [34], Syntenin (SDBP), which promotes cell invasion in multiple cancer models [35, 36], p130Cas, which is involved in focal adhesion kinase (FAK) promoted invasion [37], and Cysteine rich protein 1 (CRIP1), which is regulated by the EGFR ligand transforming growth factor-β (TGF-β) and mediates cell contractility [38]. None of these proteins have previously been specifically linked to EGFR mediated invasion. HGF specific mediators of invasion are indicated in Figure 5D. The association between these proteins and cell migration or invasion is less well

characterized, but pragmin (DKFZp761P0423) has been shown to be involved in migration of colorectal cancer cells; mutation of Y391 significantly reduced migration, yet phosphorylation of Y132 has not been characterized [39]. ADAM9, a secreted protein, increases cell invasion in human liver adenocarcinoma and uveal melanoma [40], but the role of phosphorylation of this protein is not known. Membrane protein, palmitoylated 5 (MPP5) is localized to the tight junctions of epithelial cells, although the functional role of this protein has not been elucidated [41]. Intriguingly, none of these proteins have been specifically related to Met mediated invasion. Thus, the proteins highlighted here warrant further studies to elucidate their role in growth factor mediated invasion.

CONCLUSIONS

Here we have quantified phosphotyrosine signaling following HGF or EGF stimulation at multiple time points and concentrations. These temporal phosphorylation profiles have significantly increased the site specific phosphotyrosine information pertaining to EGFR and Met signaling networks, and have highlighted common and distinct points downstream of these receptors. The integration of this temporal tyrosine phosphorylation data with the quantitative invasion data through PLSR analysis has enabled identification of network specific mediators of invasion in A549 cells. By using either a combined or two individual models of EGF and HGF mediated invasion, we have been able to extract overlapping and distinct pathways by which EGFR or c-Met may mediate invasion. Nodes which are differentially important in the two models may also offer insight into the distinct signaling pathways activated by these two receptors. The common interaction points between the networks may provide insight into the compensatory mechanisms by which Met can mediate growth and invasion in the presence of EGFR inhibitors. These same common nodes may represent potential therapeutic targets to inhibit invasion driven by either growth factor, offering a more general therapeutic mechanism that should prevent compensatory resistance. Overall, the quantitative data acquired in this study can be directly applied to the annotation of EGFR and Met signaling networks in NSCLC. Improved models of the signaling networks downstream of these receptors will enable the identification of potential therapeutic targets directly involved in invasive cancer growth.

Supplementary Material

Refer to Web version on PubMed Central for supplementary material.

Acknowledgments

The authors would like to thanks members of the White lab for helpful discussion.

Funding Sources

This work was supported by NIH grants R01CA118705, U54CA112967, U24CA159988, and 5U01CA141556-03

ABBREVIATIONS

ANXA2	Annexin A2
AUC	area under the curve
BCAR1	p130Cas
CALM1	Calmodulin
CID	Collision induced dissociation

CRIP1	Cysteine rich protein 1
DKFZP761P0423	Pragmin
EC_0	no growth factor
EC_{50}	the effective concentration that results in 50% of the maximum invasion
EC_{100}	the effective concentration that results in 100% i.e. maximum invasion
EC_{am50}	the effective concentration above EC_{100} that results in 50% of the maximum invasion
ECL	Enhanced chemiluminescence
EGF	Epidermal growth factor
EGFR	Epidermal growth factor receptor
ERK1	MAPK3
ERK	MAPK1
FAK	Focal adhesion kinase
HCD	Higher Energy Collision Dissociation
HGF	Hepatocyte growth factor
IMAC	Immobilized metal affinity chromatography
INPPL1	Ship2
ITSN2	Intersectin 2
LC-MS/MS	Liquid chromatography tandem mass spectrometry
MPP5	Membrane protein, palmitoylated 5
NSCLC	Non-small cell lung carcinoma
PC	Principal component
PLSR	Partial least squares regression
RTK	Receptor tyrosine kinase
SDBP	Syntenin
TGFb	Transforming growth factor-β
TNS3	Tensin3
VIP	Variable importance in the projection

References

1. de Larco J, Todaro G. Growth factors from murine sarcoma virus-transformed cells. Proc Natl Acad Sci U S A. 1978; 75(8):4001–4005. [PubMed: 211512]
2. Sporn MB, Roberts AB. Autocrine growth factors and cancer. Nature. 1985; 313(6005):745–747. [PubMed: 3883191]
3. Naldini L, Vigna E, Narsimhan R, Gaudino G, Zarnegar R, Michalopoulos G, Comoglio P. Hepatocyte growth factor (HGF) stimulates the tyrosine kinase activity of the receptor encoded by the proto-oncogene c-MET. Oncogene. 1991; 6(4):501–504. [PubMed: 1827664]

4. Bottaro D, Rubin J, Faletto D, Chan A, Kmiecik T, Vande Woude G, Aaronson S. Identification of the hepatocyte growth factor receptor as the c-met proto-oncogene product. Science. 1991; 251(4995):802–804. [PubMed: 1846706]
5. Naldini L, Weidner KM, Vigna E, Gaudino G, Bardelli A, Ponzetto C, Narsimhan RP, Hartmann G, Zarnegar R, K MG. Scatter factor and hepatocyte growth factor are indistinguishable ligands for the MET receptor. EMBO J. 1991; 10(10):2867–2878. [PubMed: 1655405]
6. Naldini L, Vigna E, Ferracini R, Longati P, Gandino L, Prat M, Comoglio PM. The tyrosine kinase encoded by the MET proto-oncogene is activated by autophosphorylation. Molecular and Cellular Biology. 1991; 11(4):1793–1803. [PubMed: 2005882]
7. Ponzetto C, Bardelli A, Zhen Z, Maina F, dalla Zonca P, Giordano S, Graziani A, Panayotou G, Comoglio PM. A multifunctional docking site mediates signaling and transformation by the hepatocyte growth factor/scatter factor receptor family. Cell. 1994; 77(2):261–271. [PubMed: 7513258]
8. Weidner KM, Di Cesare S, Sachs M, Brinkmann V, Behrens J, Birchmeier W. Interaction between Gab1 and the c-Met receptor tyrosine kinase is responsible for epithelial morphogenesis. Nature. 1996; 384(6605):173–176. [PubMed: 8906793]
9. Rong S, Segal S, Anver M, Resau JH, Vande Woude GF. Invasiveness and metastasis of NIH 3T3 cells induced by Met-hepatocyte growth factor/scatter factor autocrine stimulation. Proceedings of the National Academy of Sciences. 1994; 91(11):4731–4735.
10. Brinkmann V, Foroutan H, Sachs M, Weidner KM, Birchmeier W. Hepatocyte growth factor/ scatter factor induces a variety of tissue-specific morphogenic programs in epithelial cells. The Journal of Cell Biology. 1995; 131(6):1573–1586. [PubMed: 8522613]
11. Stabile LP, Lyker JS, Huang L, Siegfried JM. Inhibition of human non-small cell lung tumors by a c-Met antisense//U6 expression plasmid strategy. Gene Ther. 2004; 11(3):325–335. [PubMed: 14737093]
12. Normanno N, De Luca A, Bianco C, Strizzi L, Mancino M, Maiello MR, Carotenuto A, De Feo G, Caponigro F, Salomon DS. Epidermal growth factor receptor (EGFR) signaling in cancer. Gene. 2006; 366(1):2–16. [PubMed: 16377102]
13. Yarden Y. The EGFR family and its ligands in human cancer: signalling mechanisms and therapeutic opportunities. European Journal of Cancer. 2001; 37 Supplement 4(0):3–8. [PubMed: 11342194]
14. Marmor MD, Yarden Y. Role of protein ubiquitylation in regulating endocytosis of receptor tyrosine kinases. Oncogene. 2004; 23(11 REV. ISS. 1):2057–2070. [PubMed: 15021893]
15. Yaffe MB. Phosphotyrosine-binding domains in signal transduction. Nature Reviews Molecular Cell Biology. 2002; 3(3):177–186.
16. Hynes NE, Lane HA. ERBB receptors and cancer: The complexity of targeted inhibitors. Nature Reviews Cancer. 2005; 5(5):341–354.
17. Fischer OM, Giordano S, Comoglio PM, Ullrich A. Reactive Oxygen Species Mediate Met Receptor Transactivation by G Protein-coupled Receptors and the Epidermal Growth Factor Receptor in Human Carcinoma Cells. Journal of Biological Chemistry. 2004; 279(28):28970–28978. [PubMed: 15123705]
18. Jo M, Stolz DB, Esplen JE, Dorko K, Michalopoulos GK, Strom SC. Crosstalk between Epidermal Growth Factor Receptor and c-Met Signal Pathways in Transformed Cells. Journal of Biological Chemistry. 2000; 275(12):8806–8811. [PubMed: 10722725]
19. Engelman JA, Zejnullahu K, Mitsudomi T, Song Y, Hyland C, Park JO, Lindeman N, Gale C-M, Zhao X, Christensen J, Kosaka T, Holmes AJ, Rogers AM, Cappuzzo F, Mok T, Lee C, Johnson BE, Cantley LC, Jänne PA. MET Amplification Leads to Gefitinib Resistance in Lung Cancer by Activating ERBB3 Signaling. Science. 2007; 316(5827):1039–1043. [PubMed: 17463250]
20. Huang PH, Miraldi ER, Xu AM, Kundukulam VA, Del Rosario AM, Flynn RA, Cavenee WK, Furnari FB, White FM. Phosphotyrosine signaling analysis of sitespecific mutations on EGFRvIII identifies determinants governing glioblastoma cell growth. Molecular BioSystems. 2009; 6(7): 1227–1237. [PubMed: 20461251]
21. Huang PH, Mukasa A, Bonavia R, Flynn RA, Brewer ZE, Cavenee WK, Furnari FB, White FM. Quantitative analysis of EGFRvIII cellular signaling networks reveals a combinatorial therapeutic

strategy for glioblastoma. Proceedings of the National Academy of Sciences. 2007; 104(31): 12867–12872.

22. Bergstrom JD, Westermark B, Heldin N-E. Epidermal Growth Factor Receptor Signaling Activates Met in Human Anaplastic Thyroid Carcinoma Cells. Experimental Cell Research. 2000; 259(1): 293–299. [PubMed: 10942601]
23. Guo A, Villän J, Kornhauser J, Lee KA, Stokes MP, Rikova K, Possemato A, Nardone J, Innocenti G, Wetzel R, Wang Y, MacNeill J, Mitchell J, Gygi SP, Rush J, Polakiewicz RD, Comb MJ. Signaling networks assembled by oncogenic EGFR and c-Met. Proceedings of the National Academy of Sciences. 2008; 105(2):692–697.
24. Hammond DE, Hyde R, Kratchmarova I, Beynon RJ, Blagoev B, Clague MJ. Quantitative Analysis of HGF and EGF-Dependent Phosphotyrosine Signaling Networks. Journal of Proteome Research. 2010; 9(5):2734–2742. [PubMed: 20222723]
25. Zhang Y, Wolf-Yadlin A, Ross PL, Pappin DJ, Rush J, Lauffenburger DA, White FM. Time-resolved Mass Spectrometry of Tyrosine Phosphorylation Sites in the Epidermal Growth Factor Receptor Signaling Network Reveals Dynamic Modules. Molecular & Cellular Proteomics. 2005; 4(9):1240–1250. [PubMed: 15951569]
26. Johnson H, Del Rosario AM, Bryson BD, Schroeder MA, Sarkaria JN, White FM. Molecular characterization of EGFR and EGFRvIII signaling networks in human glioblastoma tumor xenografts. Molecular & Cellular Proteomics. 2012 In Press.
27. Wolf-Yadlin A, Kumar N, Zhang Y, Hautaniemi S, Zaman M, Kim H-D, Grantcharova V, Lauffenburger DA, White FM. Effects of HER2 overexpression on cell signaling networks governing proliferation and migration. Mol Syst Biol. 2006; 2
28. Zhang Y-W, Vande Woude GF. HGF/SF-met signaling in the control of branching morphogenesis and invasion. Journal of Cellular Biochemistry. 2003; 88(2):408–417. [PubMed: 12520544]
29. Lokman N, Ween M, Oehler M, Ricciardelli C. The Role of Annexin A2 in Tumorigenesis and Cancer Progression. Cancer Microenvironment. 2011; 4(2):199–208. [PubMed: 21909879]
30. Zhai H, Acharya S, Gravanis I, Mehmood S, Seidman RJ, Shroyer KR, Hajjar KA, Tsirka SE. Annexin A2 Promotes Glioma Cell Invasion and Tumor Progression. The Journal of Neuroscience. 2011; 31(40):14346–14360. [PubMed: 21976520]
31. Katz M, Amit I, Citri A, Shay T, Carvalho S, Lavi S, Milanezi F, Lyass L, Amariglio N, Jacob-Hirsch J, Ben-Chetrit N, Tarcic G, Lindzen M, Avraham R, Liao Y-C, Trusk P, Lyass A, Rechavi G, Spector NL, Lo SH, Schmitt F, Bacus SS, Yarden Y. A reciprocal tensin-3-cten switch mediates EGF-driven mammary cell migration. Nat Cell Biol. 2007; 9(8):961–969. [PubMed: 17643115]
32. Martuszewska D, Ljungberg Br, Johansson M, Landberg Gr, Oslakovic C, Dahlbäck Br, Hafizi S. Tensin3 Is a Negative Regulator of Cell Migration and All Four Tensin Family Members Are Downregulated in Human Kidney Cancer. PLoS ONE. 2009; 4(2):e4350. [PubMed: 19194507]
33. Birge RB, Fajardo JE, Mayer BJ, Hanafusa H. Tyrosine-phosphorylated epidermal growth factor receptor and cellular p130 provide high affinity binding substrates to analyze Crk-phosphotyrosine-dependent interactions in vitro. Journal of Biological Chemistry. 1992; 267(15): 10588–10595. [PubMed: 1375224]
34. Hiramoto-Yamaki N, Takeuchi S, Ueda S, Harada K, Fujimoto S, Negishi M, Katoh H. Ephexin4 and EphA2 mediate cell migration through a RhoG-dependent mechanism. The Journal of Cell Biology. 2010; 190(3):461–477. [PubMed: 20679435]
35. Meerschaert K, Bruyneel E, De Wever O, Vanloo B, Boucherie C, Bracke M, Vandekerckhove Jl, Gettemans J. The tandem PDZ domains of syntenin promote cell invasion. Experimental Cell Research. 2007; 313(9):1790–1804. [PubMed: 17451681]
36. Koo TH, Lee JJ, Kim EM, Kim KW, Kim HD, Lee JH. Syntenin is overexpressed and promotes cell migration in metastatic human breast and gastric cancer cell lines. Oncogene. 2002; 21(26): 4080–4088. [PubMed: 12037664]
37. Cary LA, Han DC, Polte TR, Hanks SK, Guan J-L. Identification of p130Cas as a Mediator of Focal Adhesion Kinase-promoted Cell Migration. The Journal of Cell Biology. 1998; 140(1):211–221. [PubMed: 9425168]

38. Järvinen PM, Myllärniemi M, Liu H, Moore HM, Leppäranta O, Salmenkivi K, Koli K, Latonen L, Band AM, Laiho M. Cysteine-rich protein 1 is regulated by transforming growth factor-β1 and expressed in lung fibrosis. Journal of Cellular Physiology. 2012; 227(6):2605–2612. [PubMed: 21882188]

39. Leroy, Cd; Fialin, C.; Sirvent, A.; Simon, Vr; Urbach, S.; Poncet, Jl; Robert, B.; Jouin, P.; Roche, S. Quantitative Phosphoproteomics Reveals a Cluster of Tyrosine Kinases That Mediates Src Invasive Activity in Advanced Colon Carcinoma Cells. Cancer Research. 2009; 69(6):2279–2286. [PubMed: 19276381]

40. Mazzocca A, Coppari R, De Franco R, Cho J-Y, Libermann TA, Pinzani M, Toker A. A Secreted Form of ADAM9 Promotes Carcinoma Invasion through Tumor-Stromal Interactions. Cancer Research. 2005; 65(11):4728–4738. [PubMed: 15930291]

41. Stöhr H, Molday LL, Molday RS, Weber BHF, Biedermann B, Reichenbach A, Krämer F. Membrane-associated guanylate kinase proteins MPP4 and MPP5 associate with Veli3 at distinct intercellular junctions of the neurosensory retina. The Journal of Comparative Neurology. 2005; 481(1):31–41. [PubMed: 15558731]

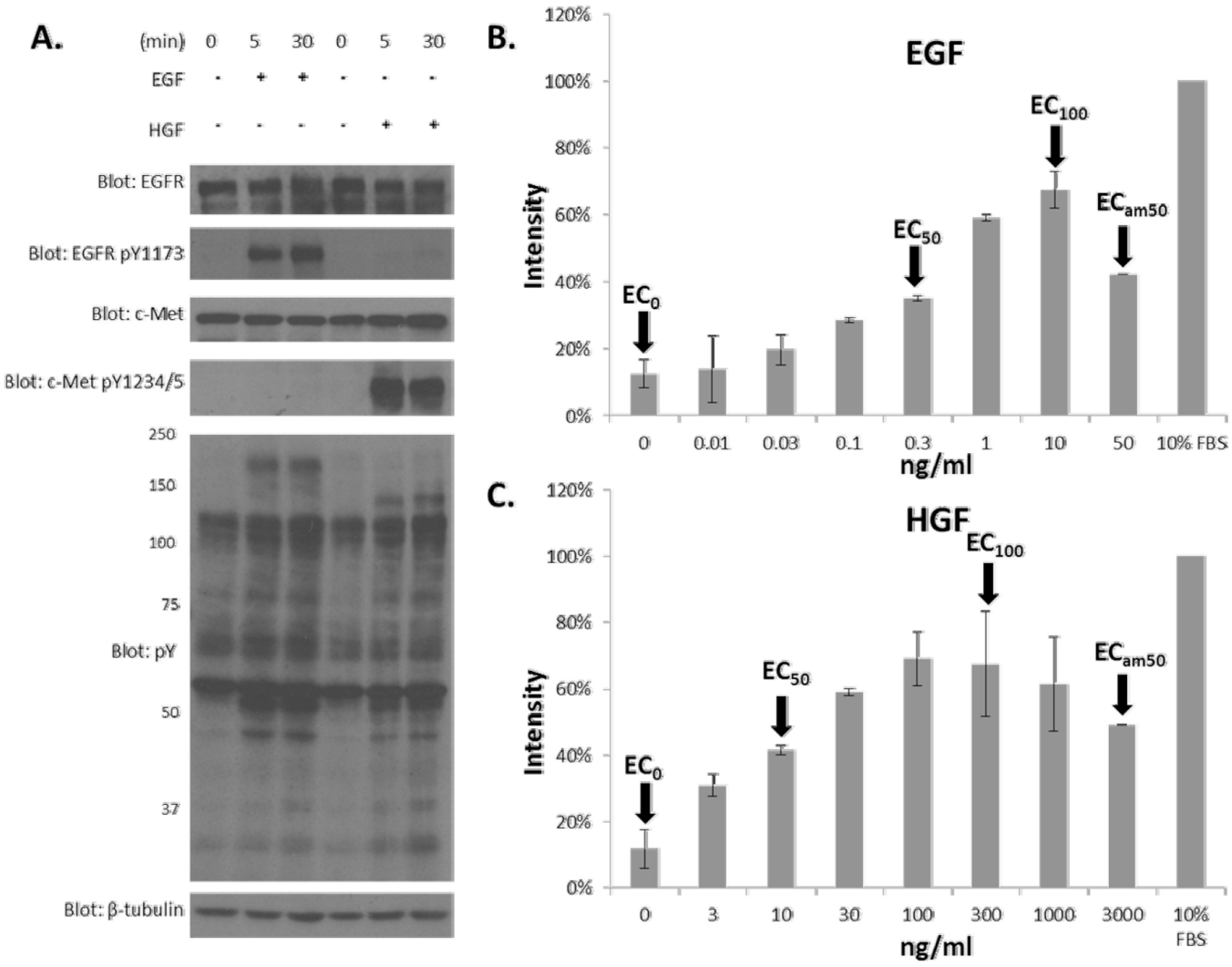

Figure 1.

EGF and HGF dose dependent stimulation of *in vitro* invasion in A549 cells. A. Immunoblotting of total EGFR, EGFR pY1173, total Met, Met pY1234/5, total phosphotyrosine (pY) and β-tubulin in A549 cells stimulated with EGF or HGF at the specified times. Immunoblots are representative of 3 biological replicates. β-tubulin is used as the loading control. B and C. Boyden chamber invasion assay of A549 cells in response to EGF and HGF, respectively at the indicated concentrations. Bar charts are representative of 2 biological replicates for all growth factor concentrations and EC_0 measurements and 4 biological replicates for 10% FBS. Error bars indicate standard error. The data were normalized to the 10% FBS condition and the EC_0, EC_{50}, EC_{100}, and EC_{am50} are indicated.

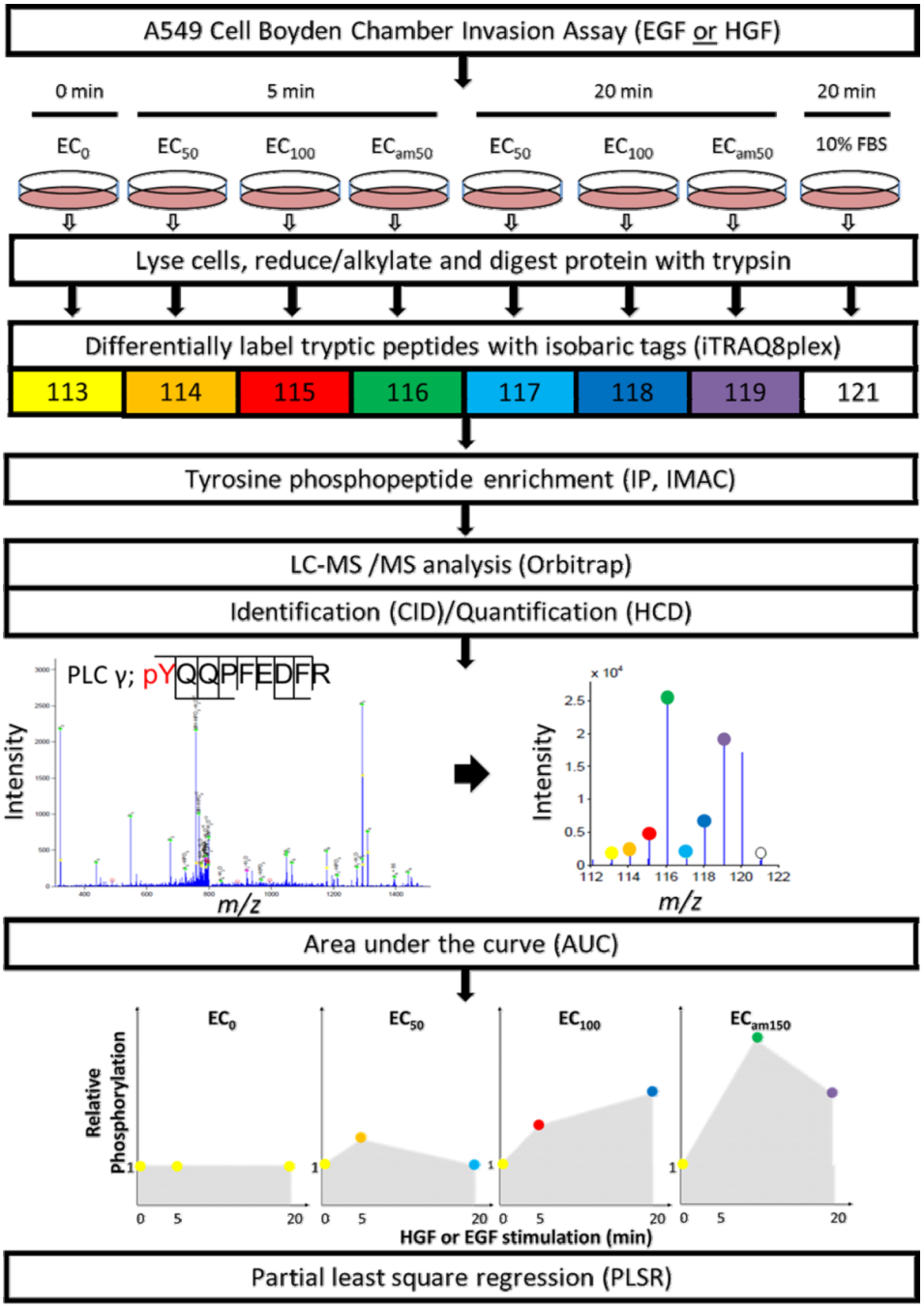

Figure 2.

Schematic diagram of the experimental mass spectrometric workflow. Effective concentrations (EC_0, EC_{50}, EC_{100} and EC_{am50}) were determined from the Boyden chamber invasion assay in response to EGF or HGF. Cells were stimulated with EGF or HGF at these concentrations for 5 or 20 minutes and cells were lysed and proteins reduced, alkylated and digested with trypsin. Peptides were then differentially labeled with iTRAQ8plex, and phosphotyrosine peptides were enriched for by immunoprecipitation using anti-phosphotyrosine antibodies and IMAC. Phosphotyrosine peptides were then analyzed by LC-MS/MS using an Orbitrap XL instrument. Peptides were identified using CID scans (left) and quantified using HCD scans (right). The AUC was calculated for each peptide at

EC_0, EC_{50}, EC_{100}, and EC_{am50} using the 5 and 20 minute time points prior to PLSR analyses.

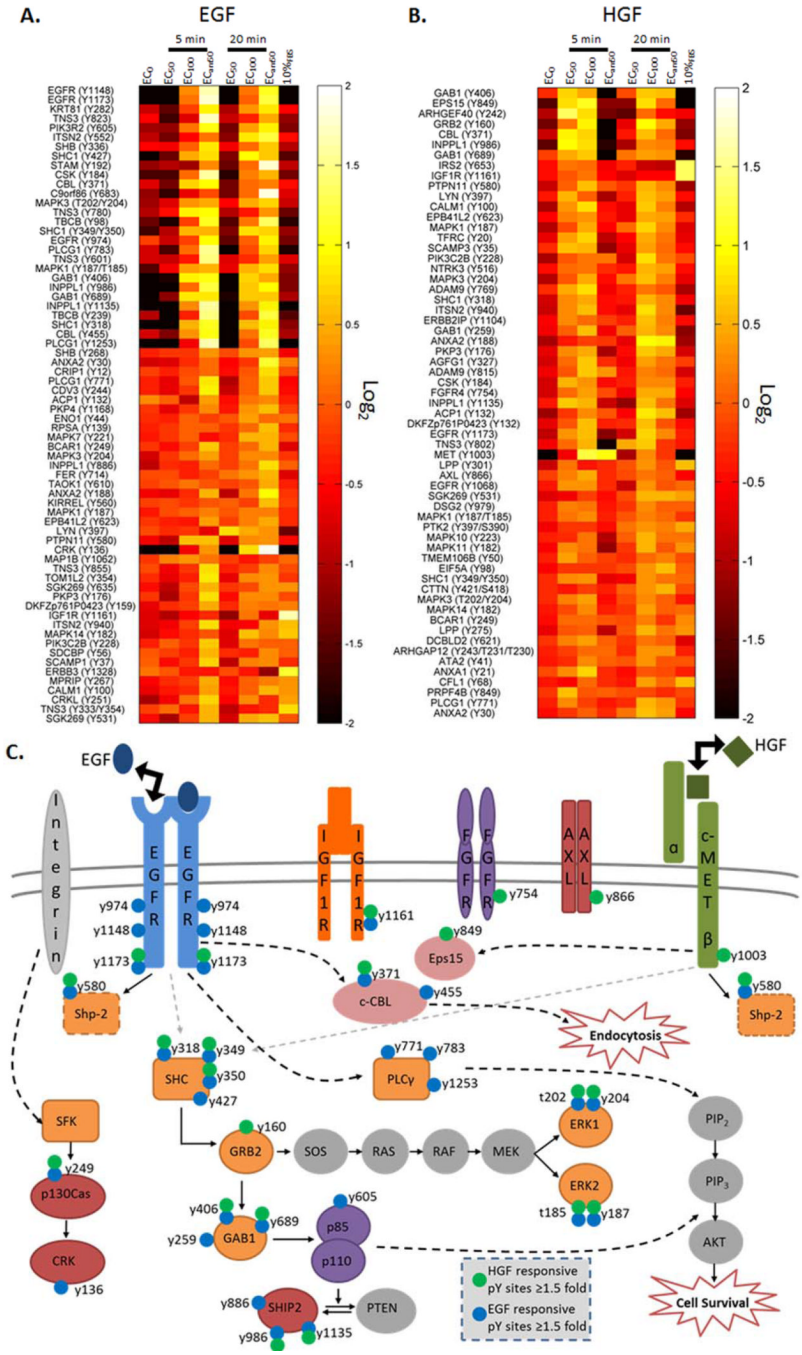

Figure 3.

Specific EGF and HGF responsive tyrosine phosphorylation sites. A. Heat map of the 68 EGF responsive phosphotyrosine peptides. B. Heat map of the 61 HGF responsive phosphotyrosine peptides. A and B, The heat maps are a representation of iTRAQ8plex fold changes normalized to the 10% FBS condition, normalized to the mean of all 8 channels and Log_2 transformed. Phosphorylation sites were clustered using affinity propagation to group sites that show similar profiles. C. EGF and HGF responsive tyrosine phosphorylation sites mapped onto a signaling network diagram. HGF responsive phosphorylation sites are indicated in green and EGF responsive phosphorylation sites are indicated in blue. The site

of phosphorylation is indicated by a lower case “y” followed by the amino acid number in the protein sequence.

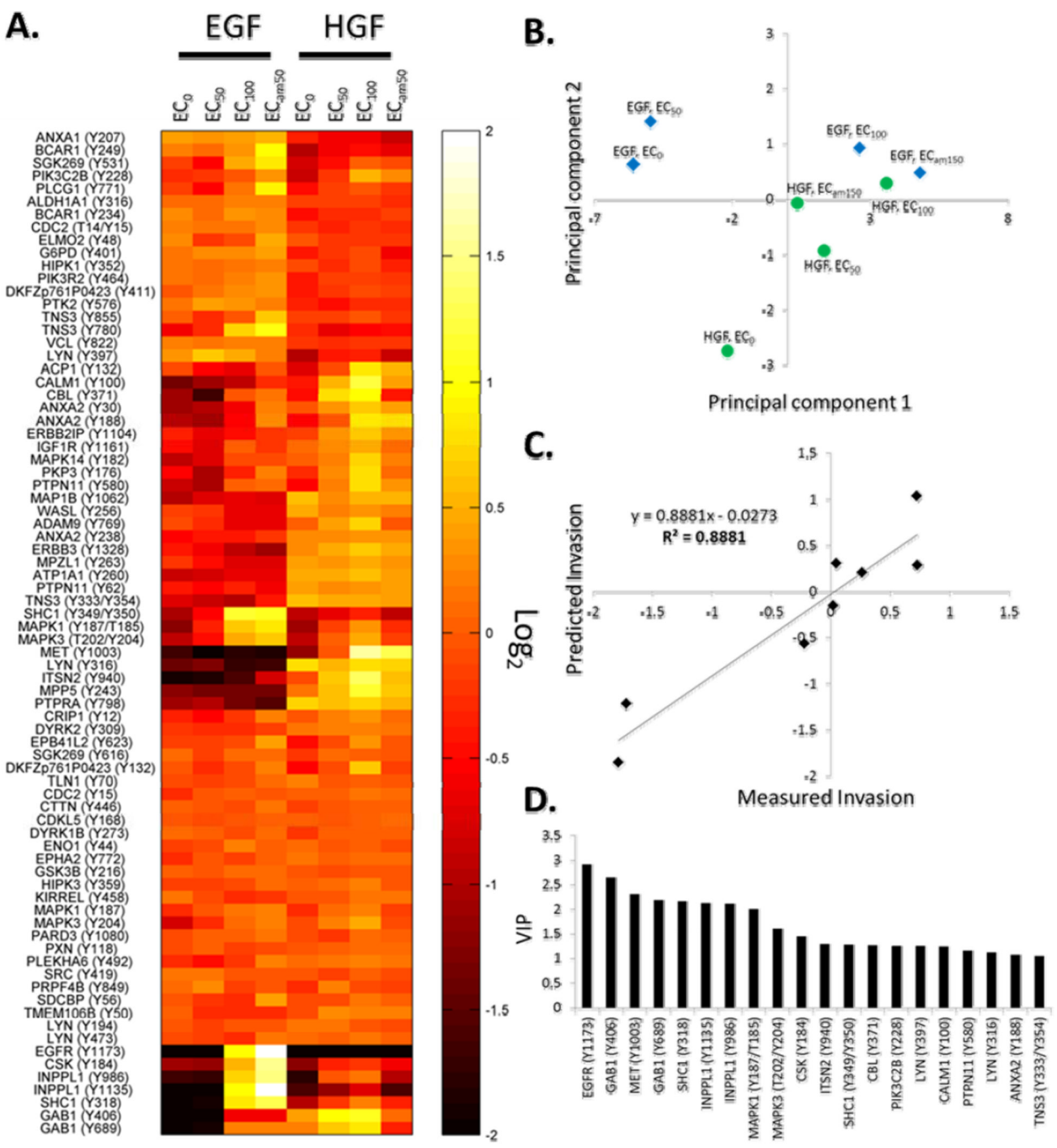

Figure 4.

Quantification and PLSR modeling of the 78 phosphorylation sites overlapping in the EGF and HGF datasets against the measured invasion in response to EGF and HGF. A. Heat map of the area under the curve of the 78 phosphotyrosine peptides quantified across HGF and EGF datasets and at EC_0, EC_{50}, EC_{100}, and EC_{am150}. B. The scores plots of the EGF and HGF combined model showing the relationship between the signaling measured in A549 cells in response to EGF and HGF stimulation in terms of principal component 1 (x-axis) vs. principal component 2 (y-axis) from a PLSR analysis of measured invasion data. The model uses 3 principal components. Growth factor conditions are color coded; EGF is blue and HGF is green. C. Plot of experimentally determined invasion (x-axis) versus predicted

invasion (y-axis) as determined by the linear EGF and HGF combined invasion model. Invasion data was normalized to the mean of all 8 conditions and Log_2 transformed. D. The bar chart displays the VIPs (Variable Importance for the Projection) for each phosphorylation site with a score above 1.

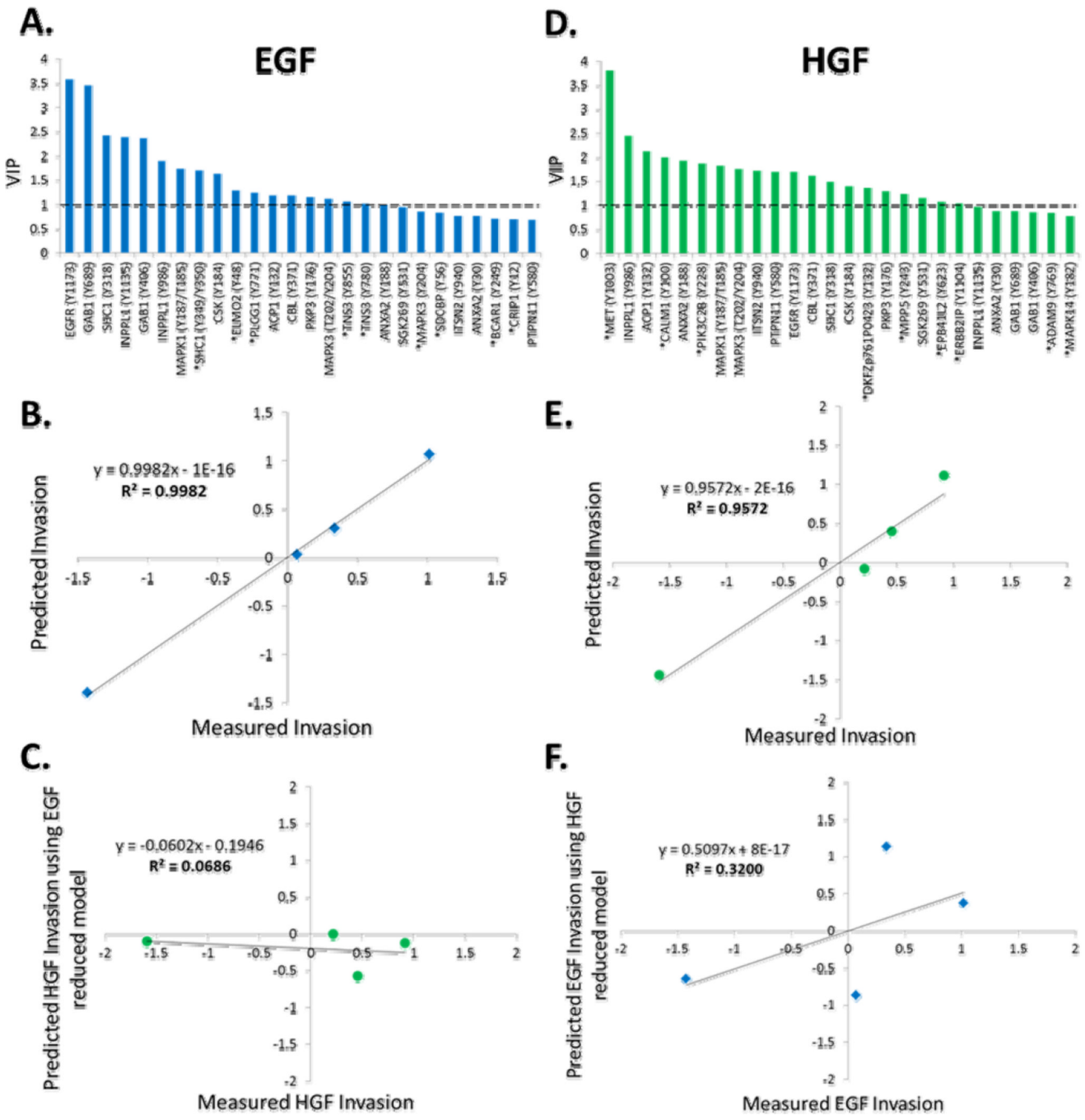

Figure 5.

Individual EGF or HGF reduced linear models predict network specific mediators of invasion. A. The bar chart displays the VIPs for the 26 most important variables from the EGF-only model. B. Plot of experimentally determined invasion (x-axis) versus predicted invasion (y-axis) as determined by the reduced linear EGF invasion model which used only the 26 phosphorylation sites to predict invasion C. Plot of experimentally determined HGF invasion at 4 growth factor concentrations (x-axis) versus predicted invasion (y-axis) as determined by the reduced linear EGF invasion model. D. The bar chart displays the VIPs for the 26 most important variables from the HGF-only model. E. Plot of experimentally determined invasion (x-axis) versus predicted invasion (y-axis) as determined by the

reduced linear HGF invasion model. F. Plot of experimentally determined EGF invasion at 4 growth factor concentrations (x-axis) versus predicted invasion (y-axis) as determined by the reduced linear HGF invasion model. Blue data points and bars indicate EGF data and green data points and bars indicate HGF data. A and D The dotted line indicates the score of 1 and asterisks indicate phosphorylation sites specific to each model.